Chalcogenide Letters Vol. 22, No. 6, June 2025, p. 551 - 560

Quaternary chalcogenides as transport layers in solid-state DSSC: a feasibility study

M. H. Ibrahim *, M. R. Salim, M. Y. Mohd Nor, A. S. Abdullah, A. I. Azmi
Lightwave Communication Research Group, Faculty of Electrical Engineering, Universiti Teknologi Malaysia, 81310 Johor, Malaysia

Four chalcogenide compounds: copper zinc germanium sulfide (CZGS), copper zinc germanium selenide (CZGSe), copper barium tin sulfide (CBTS), and copper manganese tin sulfide (CMTS) were proposed as hole transport layer (HTL) in dye-sensitized solar cell (DSSC). The DSSC structure comprises fluorine-doped tin oxide (FTO) as the top electrode, zinc oxysulfide (ZnOS) as the electron transport layer (ETL), N719 dye as the light absorber, chalcogenides as the HTL, and gold (Au) as the back electrode. By utilizing the SCAPS 1-D simulator, the optimal thicknesses for ZnOS, HTL candidates and N719 dye were determined to be 50 nm, 200 nm, and 700 nm, respectively. Among the materials studied, CZGSe demonstrated the highest power conversion efficiency (PCE) at 12.11%, followed by CZGS and CBTS at 12.02%. In contrast, CMTS exhibited a significantly lower PCE of 4.25%, indicating its limited suitability for DSSC applications. The DSSC exhibited stable performance, with PCE fluctuations constrained within 0 to 0.4%, even as the hole transport layer (HTL) varied in thickness between 50 nm and 300 nm. Comparative analysis with published simulation and experimental studies supports the promising potential of quaternary chalcogenides in solid-state DSSC applications.

(Received March 9, 2025; Accepted June 23, 2025)

Keywords: Quarternary chalcogenide, Dye-sensitized, Solar cells, Transport layer

1. Introduction

Solar energy, recognized as a sustainable and abundant power source, has garnered significant attention in recent years, driven by the continuous decline in fossil fuel reserves and the urgent need for cleaner, renewable alternatives to meet global energy demands. In tropical countries, the abundance of sunlight throughout the year further promotes the adoption of solar energy. One of the key technologies harnessing solar power for electricity generation is solar cells. Generally, there are three generations of solar cells, each with distinct features. In the first generation, which is a silicone-based solar cell, it can be categorised as mono and poly-crystalline. It is the most established and widely used solar cells, accounting for most of the commercial market. Thin-film solar cells of the second generation encompass materials such as gallium arsenide, cadmium telluride, and amorphous silicon. In contrast, third-generation technologies include dye-sensitized, perovskite, and organic solar cells [1].

The dye-sensitized solar cell (DSSC) emerged in 1991, pioneered by O'Regan and Grätzel [2]. This innovation provided an alternative route for solar energy harvesting. It consists of an electron transport layer (ETL) that accommodates a monolayer of photosensitizer, accompanied by an electrolyte and a counter electrode. Since then, it has attracted significant research interest and rapid development due to its huge advantages, including economical in costs, adaptable architectures and less-complex fabrication [3-4]. In a typical DSSC, ruthenium-based dye, which is commonly used as sensitizer, absorb sunlight and generate excited electrons, contributing to electrical energy generation. These electrons complete the circuit by moving through the ETL, front contact, external load, and back electrode, eventually being restored by the redox electrolyte [5]. Due to its advantages in terms of optical properties, abundance and non-hazardous, titanium dioxide (TiO_2) has been widely used as the ETL in DSSCs [6–8]. Alternatively, various metal oxides have been researched and applied as the ETL to address the problem of hysteresis-related energy losses and limited device

* Corresponding author: mohdhaniff@utm.my
https://doi.org/10.15251/CL.2025.226.551

lifetimes. Studies by Korir and co-workers [6], Shixuan and co-workers [9] and Haoliang et al. [10], have demonstrated the viability of zinc oxysulfide (ZnOS), zinc oxide (ZnO), and tin oxide (SnO_2) as ETL materials in DSSCs.

The main element that makes the DSSC recyclable is the electrolyte. Research on the tri-iodide redox pair, disulphide/thiolate redox couple, and other organic-based redox couples [11-13] have extensively demonstrated the usage of standard liquid electrolyte in DSSC. However, as noted by Wu and co-workers [14], liquid electrolytes are prone to issues such as solvent volatilization, leakage, photodegradation, and counter electrode corrosion. These elements collectively pose significant challenges to the durability and sustained performance of DSSC. Consequently, various efforts have focused on substituting liquid-based redox electrolytes with solid-state alternatives, commonly referred to as the hole transport layer (HTL). In a prior study, Korir and his colleagues replaced the liquid electrolyte with copper thiocyanate (CuSCN), a solid-state p-type material [15]. However, as viable alternatives to the conventional liquid electrolyte, Li et al. [8] suggested combining copper iodide (CuI), polymeric-based Spiro-OMeTAD and p-type copper thiocyanate (CuSCN). Another effort by Chakraborty and his colleagues [16] had utilised a polymer doped graphene oxide as a possible electrolyte substitution in solid-state DSSC.

Quaternary chalcogenides, also known as kesterite is a subset of chalcogenide and contain four different elements, which typically include metals and chalcogens (Group 16 of periodic table). They have been previously used as solar cell absorbers, as demonstrated by Qing et al. [17], Benmir et al. [18] and Messei et al. [19]. These materials are promising for solar applications due to huge advantages which include cost-effective, naturally abundant, and structurally stable [20]. Meanwhile, these chalcogenides have been previously applied as a transport layer in perovskite solar cell application. For instance, work by Bouhjar et al. [21] on copper zinc tin sulfide (CZTS) HTL and copper zinc tin selenide (CZTSe) which was simulated by Dixit and colleagues in 2023 [22]. Additionally, simulation work by Khan and co-workers [23] on lead-free perovskite solar cells had adopted the HTL based on several chalcogenide compounds which include CZTSe, copper nickel tin sulfide (CNTS), copper ferum tin sulfide (CFTS), and CZTS. Some studies have also demonstrated the effectiveness of chalcogenide compounds as counter electrodes in dye-sensitized solar cells (DSSCs) [24-25]. As per our understanding, research on employing quaternary chalcogenide as an HTL for DSSCs remains unexplored. In this study, we aim to investigate the feasibility of this class of material, motivated by its prior success in perovskite solar cells.

This paper will briefly explain on the possible application of four chalcogenide compounds as the solid-state HTL in DSSC. The proposed structures will be based on N719 dye as the light absorber and ZnOS as the ETL. SCAPS 1-D, widely used in solar cell simulation research and proven to yield promising results [26-27], will be employed for the numerical simulation of the proposed structure. Its reliability in producing consistent outcomes further supports its selection for this study. Although this study is based solely on simulations, the promising findings may provide critical perspectives for refining and advancing solid-state DSSC technology.

2. Simulation methods

In this work, the SCAPS 1-D simulator [28] will be our primary tool for solving the hole concentration, electron concentration, and electrostatic potential in the solar cell analysis. The electrostatic potential analysis, which is one-dimensional (1-D) with respect to the spatial coordinate, requires solving Poisson's equation in equation (1), while the electron and hole continuity equations are represented by equations (2) and (3) and (4) and (5), respectively. The internal generation of the solar illumination model in this work occurs at AM 1.5 G (1000 Wm^{-2}).

$$\frac{d^2\varphi(X)}{dX^2} = -\frac{\partial E}{\partial X} = -\frac{p}{\varepsilon_s} = -\frac{q}{\varepsilon_s}\left[p - n + N_D^+(X) - N_a^+(X) \pm N_{def}(X)\right] \quad (1)$$

$$-\frac{\partial J_p}{\partial X} + G - U_p(n,p) = 0 \quad (2)$$

$$J_p = qn\mu_p E + qD_p \frac{\partial p}{\partial X} \quad (3)$$

$$\frac{\partial J_n}{\partial X} + G - U_n(n,p) = 0 \quad (4)$$

$$J_n = qn\mu_n E + qD_n \frac{\partial n}{\partial X} \quad (5)$$

The stated parameters in equations (1–5) are described as: Relative permittivity is represented by ε_s, electric potential by φ, hole current density by J_p, electron-hole generation rate by G, elementary charge by q, recombination rates by U_n/U_p, electron density by n, electron diffusion coefficient by D_n, hole diffusion coefficient by D_p, hole density by p, ionized donor density by N_D^+, ionized acceptor density by N_a^+, electron current density by J_n, electron mobility by μ_n, and hole mobility by μ_p.

A cross-sectional depiction of the DSSC design is displayed in Fig. 1. Within this arrangement, fluorine-doped tin oxide (FTO) serves as the transparent conductive electrode, while ZnOS is utilized as the ETL. For the hole transport layer candidate, four quaternary chalcogenides: copper zinc germanium sulfide (CZGS), copper zinc germanium selenide (CZGSe), copper barium tin sulfide (CBTS), and copper manganese tin sulfide (CMTS) are integrated with an N719 dye, which serves as the photosensitizer. Gold (Au) is to serve as the basis for a counter electrode. Table 1 provides an overview of the materials, and their corresponding properties incorporated into our simulation. The selection of these properties was based on reputable literature sources [6, 29–30]. Meanwhile, Figs. 2(a–d) depict the energy level diagrams for the layer interfaces, which were developed using the initial layer dimensions specified in Table 1. The valence band offset (VBO) and conduction band offset (CBO) have been calculated based on the use of Anderson's Rule [31], which further justifies the selection of ZnOS as the ETL and the proposed quaternary chalcogenide candidates as the solid-state HTL.

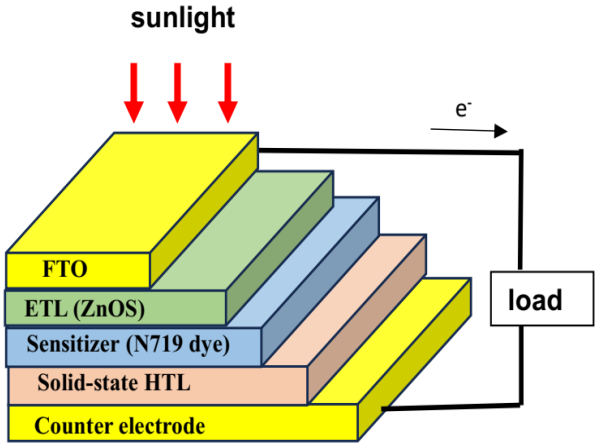

Fig. 1. Basic architecture of proposed DSSC.

Table 1. Properties of materials used in solid-state DSSCs with chalcogenide candidates.

Properties	FTO	ZnOS	N719 dye	CZGS	CZGSe	CBTS	CMTS
Thickness(nm)	400	50	400	200	200	200	200
Bandgap (eV)	4.5	2.83	2.93	1.8	1.4	1.9	1.6
Affinity (eV)	4.0	3.6	3.9	3.67	4.1	3.6	4.35
Dielectric Permittivity	9	9	30	10	8.42	5.4	9
DOS_{CB} (cm^{-3})	$2.2x10^{18}$	$2.2x10^{18}$	$2.4x10^{20}$	$2.2x10^{18}$	$2.2x10^{18}$	$2.2x10^{18}$	$2.2x10^{18}$
DOS_{VB} (cm^{-3})	$1.8x10^{19}$	$1.8x10^{18}$	$2.5x10^{20}$	$1.8x10^{19}$	$1.8x10^{19}$	$1.8x10^{19}$	$1.8x10^{19}$
μ_e (cm^2/Vs)	20	100	5	60	60	30	0.16
μ_h (cm^2/Vs)	10	25	5	20	20	10	0.16
Acceptor Concentration (cm^{-3})	0	0	$1x10^{17}$	$1x10^{19}$	$1x10^{19}$	$1x10^{19}$	$1x10^{19}$
Donor Concentration (cm^{-3})	$2x10^{19}$	$2x10^{18}$	0	0	0	0	0
Defect Density (cm^{-3})	0	$1x10^{14}$	$5x10^{16}$	$1x10^{14}$	$1x10^{14}$	$1x10^{14}$	$1x10^{14}$

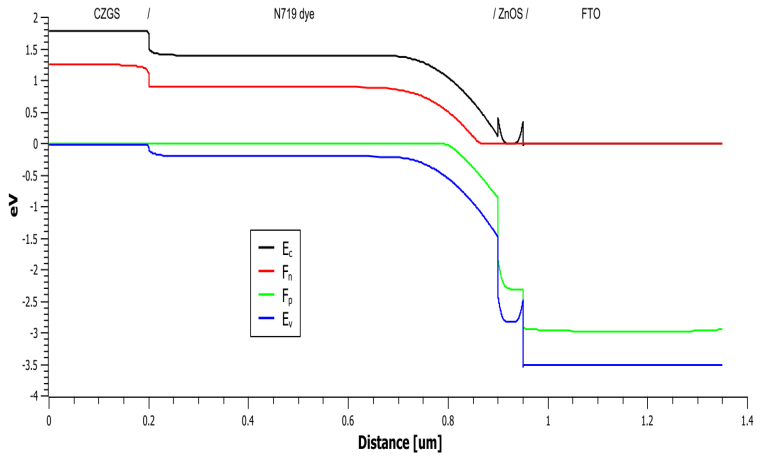

(a)

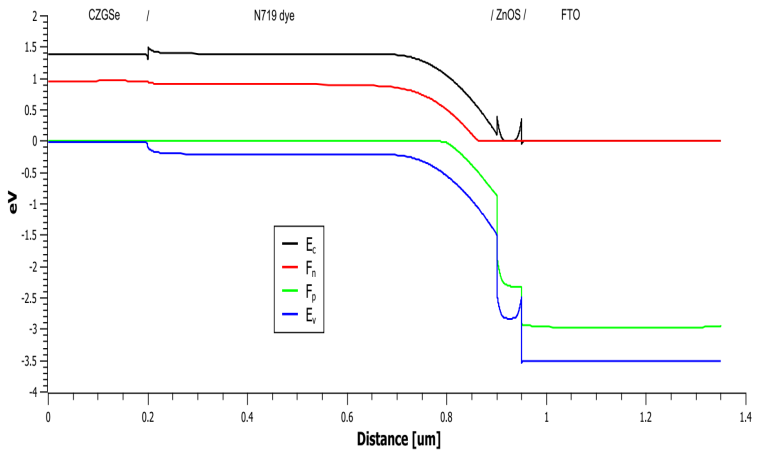

(b)

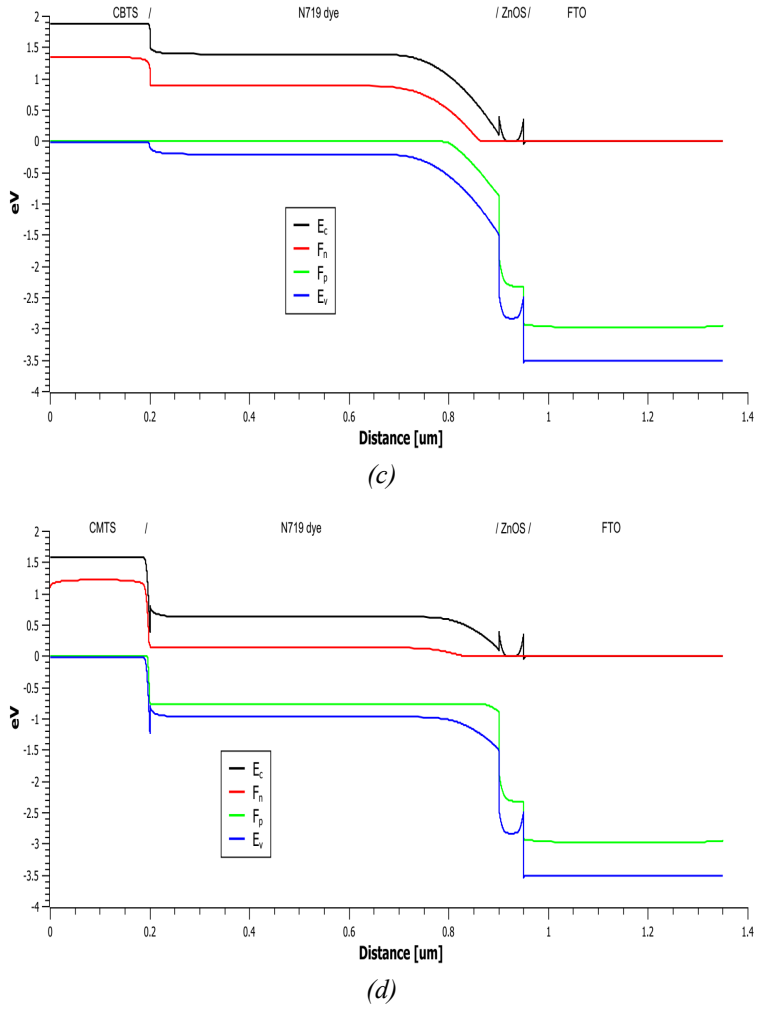

Fig. 2. Energy band diagrams of the designed solid-state DSSC.

We shall change the N719 dye's thickness in the first stage of this study from 50 to 900 nm. With the thickness of the HTL chosen at 200 nm, this modification will aid in determining how the N719 dye absorber affects the functionality of our proposed chalcogenide-based DSSC. Furthermore, we will adjust the chalcogenide thickness within the range of 50–300 nm and assess the efficiency parameters of the DSSC while maintaining a fixed thickness for the photosensitizer and ETL. The performance of our suggested structure will then be compared with solid-state DSSC structures (simulation and experimental based) that have been previously proposed [6, 32-36]

3. Results and discussion

Using the parameters from Table 1, simulations were conducted on four chalcogenide candidates: CGZS, CGZSe, CBTS, and CMTS. It is worth noting that the thicknesses of these chalcogenides and ZnOS were fixed at 200 nm and 50 nm, respectively, for this simulation. Fig. 3 illustrates the impact of N719 dye thickness variations (50–900 nm) on the simulated power conversion efficiency (PCE).

It is observed that up to 250 nm, the values for CZGS, CZGSe, and CBTS increase proportionally with dye thickness before stabilizing at 650 nm and beyond. CMTS, on the other hand, shows significant fluctuations in PCE between 50 and 400 nm before stabilizing at 700 nm and beyond. Fundamentally, the number of photo-generated electrons captured by ZnOS in its conduction band should increase substantially as the dye thickness grows. However, the results

indicate that beyond a certain threshold, further increases in dye thickness may not significantly impact the simulated PCE. Since a thickness of 700 nm closely aligns with the stable PCE values for all kesterite candidates, it is adopted as the optimal N719 dye thickness in this study.

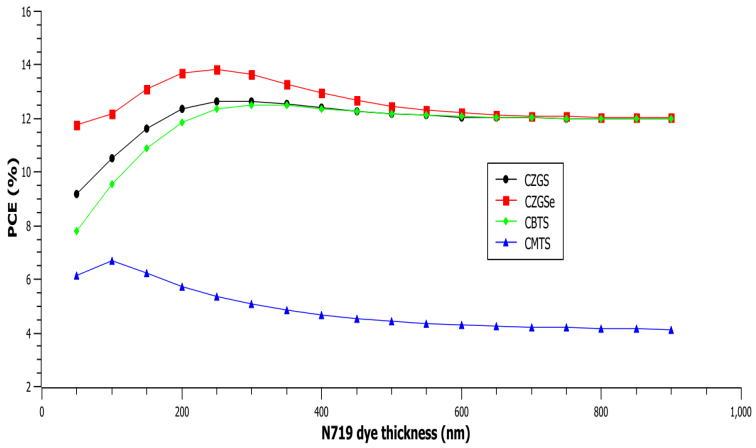

Fig. 3. PCE variation with N719 dye thickness for constant HTL thickness.

Secondly, we adjusted the HTL thickness within the range of 50–300 nm, maintaining the N719 dye and ZnOS thicknesses at fixed values of 700 nm and 50 nm, respectively. Fig. 4 presents the simulation results, which indicate that within this range, variations in chalcogenide thickness result in an essentially stable PCE. The percentage changes for CZGS, CZGSe, CBTS, and CMTS are 0%, 0.14%, 0%, and 0.4% respectively. This finding suggests that DSSC operation remains stable across a range of HTL thicknesses. Notably, it aligns with previously reported studies on solid-state HTLs for DSSCs, such as the work by Korir and his co-workers [15] on CuSCN electrolytes.

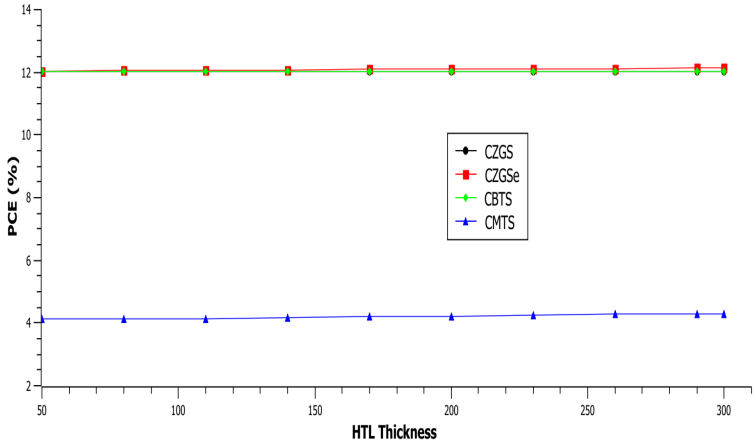

Fig. 4. PCE variation with chalcogenide thickness.

The performance metrics of the DSSC with our proposed chalcogenide HTL can be analyzed based on the simulated J-V curves shown in Fig. 5. The curves were generated based on the optimal thickness values: 700 nm for the N719 dye, 50 nm for ZnOS, and 200 nm for the chalcogenide layer. The findings highlight that among the examined materials, CZGSe achieves the highest PCE of 12.11%. This performance is associated with an open-circuit voltage (V_{oc}) of 0.8722 V, a short-circuit current density (J_{sc}) of 19.53 mA/cm², and a fill factor (FF) of 71.08%. Conversely, the DSSC

incorporating CMTS as the HTL demonstrates the lowest PCE of 4.25% and an FF of 40.98%, supplemented by a V_{oc} of 0.8947 V and a J_{sc} of 11.59 mA/cm².

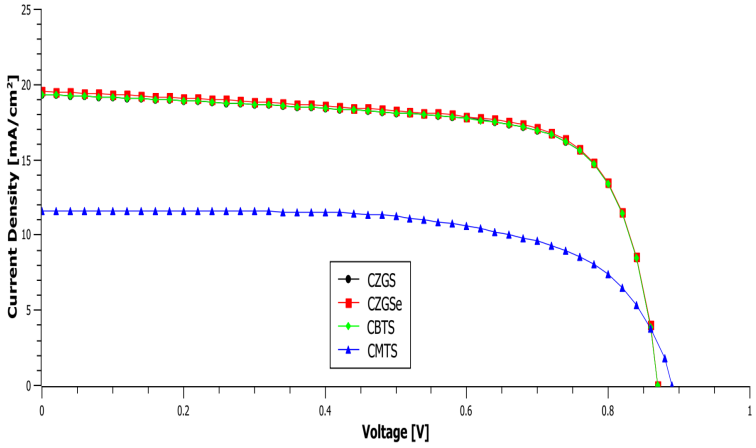

Fig. 5. J-V curves for different HTL candidates.

Fig. 6 illustrates the simulated IPCE (incident photon to current conversion efficiency) responses for the designed structures. The illumination wavelength was selected within the visible spectrum range. Evidently, for solid-state DSSCs with CZGS, CZGSe, and CBTS chalcogenides, the curves increase from an average value of 50% to an optimal average value of 96% at a wavelength of 360 nm. These findings justify the high PCE values for these HTL candidates. Despite this, the CMTS curve indicates a much smaller IPCE percentage, with an optimal value of 26.88% at 540 nm. This simulated result supports the low PCE value for CMTS-based DSSCs. Nevertheless, we have demonstrated that the adoption of quaternary chalcogenides as solid-state HTLs in DSSCs improves carrier generation, as minor photon to current conversion was observed up to a wavelength of 880 nm. This enhancement is particularly notable when compared to solid-state DSSC without an HTL, such as in the work of Korir et al. [6], where a non-zero IPCE percentage was recorded only up to 770 nm.

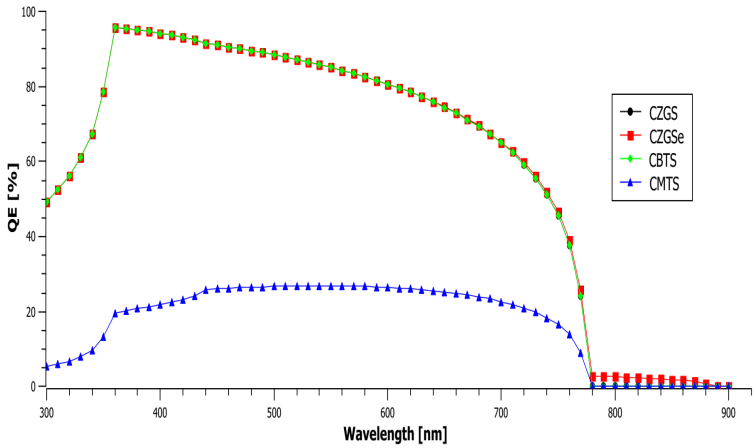

Fig. 6. IPCE curves for DSSCs with respective HTL candidates.

In the final section of this study, a brief comparison with previously published work on solid-state HTL DSSCs is presented. For a fair comparison, a few simulations and experimental studies have been selected, as summarized in Table 2. Based on these results, our proposed solid-state DSSC with quaternary chalcogenide candidates demonstrates promising conversion efficiency, which can be further improved with slight refinements in material selection. Notably, CMTS exhibited significantly lower PCE compared to other candidates, which may limit its practical application in solid-state DSSC development.

Table 2. Comparison of conversion efficiency with published work.

Solar cell structure	Mode of study	PCE [%]
FTO/TiO_2/N719 dye/Au [6]	simulation	10.22
FTO/ZnOS/N719 dye/Au [6]	simulation	11.52
FTO/TiO_2/BEHP-co-MEH PPV/PEDOT:PSS/Pt [32]	simulation	7.95
FTO/TiO_2/BEHP-co-MEH PPV/MoO_2MoO_3/Pt [32]	simulation	8.42
FTO/TiO2/N719/CuI/Au [33]	simulation	17.72
FTO/TiO2/N719/CuSCN/ Au [33]	simulation	16.69
FTO/TiO_2/LEG4 dye/PEDOT/Ag [34]	experimental	7.11
FTO/TiO_2/N719 dye/PMMA gel/Pt-FTO [35]	experimental	4.68
FTO/TiO2/N3 dye/Polymer blend gel/Pt-FTO [36]	experimental	5.43
FTO/ZnOS/N719 dye/CZGS/Au [this work]	simulation	12.02
FTO/ZnOS/N719 dye/CZGSe/Au [this work]	simulation	12.11
FTO/ZnOS/N719 dye/CBTS/Au [this work]	simulation	12.02
FTO/ZnOS/N719 dye/CMTS/Au [this work]	simulation	4.25

4. Conclusion

By applying SCAPS 1-D simulator, we investigated the feasibility of four quaternary chalcogenide candidates: CZGS, CZGSe, CBTS and CMTS as solid-state HTL in DSSCs. These materials were examined as alternatives to traditional liquid electrolytes, paired with Au as the counter electrode, FTO as the photoelectrode, N719 dye as the photosensitizer, and ZnOS as the ETL. Our findings indicate that the highest PCE of 12.11% was achieved with a CZGSe thickness of 200 nm, along with 50 nm of ZnOS and 700 nm of N719 dye. This finding is additionally confirmed by QE and J-V characteristics, which indicate light absorption reaching 880 nm in the case of CZGSe. Additionally, we demonstrated that varying the thickness of the proposed HTLs between 50 and 300 nm (while maintaining the thickness for other layers) resulted in minimal fluctuations in PCE, with a variation range of 0% to 0.4%. For comparison, a few published results have been summarized, further supporting our findings that these quaternary chalcogenides hold promise as efficient transport layers for solid-state DSSC technology.

Acknowledgements

This research was funded entirely by Universiti Teknologi Malaysia through the Potential Academic Staff (PAS) grant no. Q.J130000.2723.03K85. The authors sincerely appreciate Dr. Marc Burgelman from the University of Ghent for granting access to the SCAPS-1D simulation tool.

References

[1] K. Ranabhat, L. Patrikeev, A. Antal'evna, K. Andrianov, V. Lapshinsky, E. Sofronova, Journal of Applied Engineering Sciences, 14(4), 481 (2016); https://doi.org/10.5937/jaes14-10879

[2] B. O'Regan, M. Gratzel, Nature, 353, 737 (1991); https://doi.org/10.1038/353737a0

[3] W.R. Erwin, H.F. Zarick, E.M. Talbert, R. Bardhan, Energy & Environmental Science, 9, 1507 (2016); https://doi.org/10.1039/C5EE03847B

[4] J. Gong, K. Sumathy, Q. Qiao, Z. Zhou, Renewable and Sustainable Energy Reviews , 68, 234 (2017); https://doi.org/10.1016/j.rser.2016.09.097

[5] M.Q. Lokman, S. Shafie, S. Shaban, F. Ahmad, H. Jaafar, R. Mohd Rosnan, H. Yahaya, S.S. Abdullah, Materials, 12, 2111 (2019); https://doi.org/10.3390/ma12132111

[6] B.K. Korir, J.K. Kibet, S.M. Ngari, Journal of Electronic Materials, 50, 7259 (2021); https://doi.org/10.1007/s11664-021-09250-7

[7] F.O. Lenzmann, B.C. O'Regan, J.J.T. Smits, H.P.C.E. Kuipers, P.M. Sommeling, L.H. Slooff J.A.M. van Roosmalen, Progress in Photovoltaics: Research and Applications, 13, 333 (2005); https://doi.org/10.1002/pip.631

[8] M. Li, Z.-K. Wang, Y.-G. Yang, Y. Hu, S.-L. Feng, J.-M. Wang, X.-Y. Gao, L.-S. Liao, Advanced Energy Materials, 6(21), 1601156 (2016); https://doi.org/10.1002/aenm.201601156

[9] X. Shixuan, F. Dong, X. Fengming, R. Yuxuan, B. Chen, M. Baoxiu, G. Zhiqiang, Journal of Solid State Electrochemistry, 28(2), 589 (2024).

[10] C. Haoliang, L. Yawen, C. Bin, C. Hagglund, T. Kubart, G. Boschloo, T. Haining, ACS Applied Energy Materials, 5(10), 12022 (2022); https://doi.org/10.1021/acsaem.2c01328

[11] H. Kusama, H. Arakawa, Solar Energy Materials and Solar Cells, 85(3), 333 (2005); https://doi.org/10.1016/j.solmat.2004.05.003

[12] Z. Zhang, P. Chen, T.N. Murakami, S.M. Zakeerudin, M. Gratzel, Advanced Functional Materials, 18(2), 341 (2008); https://doi.org/10.1002/adfm.200701041

[13] C. Ming, Y. Xichuan, L. Shifeng, W. Xiuna, S. Licheng, Energy & Environmental Science, 5(4), 6290 (2012).

[14] J. Wu, Z. Lan, S. Hao, P. Li, J. Lin, M. Huang, L. Fang, Y. Huang, Pure and Applied Chemistry, 80(11), 2241 (2008); https://doi.org/10.1351/pac200880112241

[15] B.K. Korir, J.K. Kibet, S.M. Ngari, Optical and Quantum Electronics, 53, 368 (2021); https://doi.org/10.1007/s11082-021-03013-8

[16] N. Chakraborty, R. Sharma, R.K. Singh, S.K. Mukherjee, N. Sharma, Nano, 17(4), 225015 (2022); https://doi.org/10.1142/S1793292022501156

[17] Z. Qing, C. Yijia, L. Hao, W. Tingchun, X. Yuchen, Y. Xiaobing, T. Xiaoyun, G. Chao, S. Yali, Y. Wei, Materials Today Energy, 46, 101730 (2024); https://doi.org/10.1016/j.mtener.2024.101730

[18] A. Benmir, M. L. Louazene, Chalcogenide Letters, 21(4), 305 (2024); https://doi.org/10.15251/CL.2024.214.305

[19] N. Messei, M.S. Aida, A. Attaf, N. Hamani, S. Laznek, Chalcogenide Letters, 20(2),165 (2023); https://doi.org/10.15251/CL.2023.202.165

[20] B. Bibi, B. Farhadi, W. Ur Rahman, A. Liu, Next Materials, 2, 100068 (2024); https://doi.org/10.1016/j.nxmate.2023.100068

[21] F. Bouhjar, L. Derbali, Y.H. Khattak, B. Mari, Optical Materials, 147, 114582 (2024); https://doi.org/10.1016/j.optmat.2023.114582

[22] H. Dixit, N.K. Bansal, S. Porwal, D. Kumar, T. Singh, Optik, 295, 171474 (2023); https://doi.org/10.1016/j.ijleo.2023.171474

[23] A.H.H. Khan and A.A. Khan, Inorganic Chemistry Communications, 174, 114007 (2025); https://doi.org/10.1016/j.inoche.2025.114007

[24] S.K. Swami, N. Chaturverdi, A. Kumar, V. Dutta, Electrochimica Acta, 263, 26 (2018); https://doi.org/10.1016/j.electacta.2018.01.030

[25] M. Soltanmohammadi, V. Karimi, S. Alee, M. Abrari, M. Ahmadi, M. Ghanaatshoar, Semiconductor Science and Technology, 36(10), 105008 (2021); https://doi.org/10.1088/1361-6641/ac1962

[26] N.A. Buruhanutheen, A.S. Abdullah, M.H.I. Ibrahim, F. Ahmad, M.H. Ibrahim, Photonics Letters of Poland, 15(3), 45 (2023); https://doi.org/10.4302/plp.v15i3.1231

[27] A.I. Azmi, M.Y. Mohd Noor, M.H.I. Ibrahim, F. Ahmad, M.H. Ibrahim, Jordan Journal of Electrical Engineering, 8(4), 355 (2022); https://doi.org/10.5455/jjee.204-1659340463

[28] M. Burgelman, K. Decock, S. Khelifi and A. Abass, Thin Solid Films, 535, 296 (2013); https://doi.org/10.1016/j.tsf.2012.10.032

[29] A.C. Benisha, S. Routray, Y. Massoud, Optical Materials, 133, 112975 (2022); https://doi.org/10.1016/j.optmat.2022.112975

[30] Z. Khan, M. Noman, S.T. Jan, A.D. Khan, Solar Energy, 257, 58 (2023); https://doi.org/10.1016/j.solener.2023.04.019

[31] R.L. Anderson, IBM Journal of Research and Development , 4, 283 (1960); https://doi.org/10.1147/rd.43.0283

[32] V. Rondan-Gomez, F. Ayala-Mato, D. Seuret-Jimenez, G. Santana-Rodriguez, A. Zamudio-Lara, I. Montoyo De Los Santos, H.Y. Seuret-Hernandez, Optical and Quantum Electronics., 52, 324 (2020); https://doi.org/10.1007/s11082-020-02437-y

[33] F. Jahantigh, M.J. Safikhani, Applied Physics A, 125, 276 (2019); https://doi.org/10.1007/s00339-019-2582-0

[34] J. Zhang, N. Vlachopoulos, M. Jouini, M.B. Johansson, X. Zhang, M.K. Nazeeruddin, G. Boschloo, E.M.J. Johansson, A. Hagfeldt, Nano Energy, 19, 455 (2016); https://doi.org/10.1016/j.nanoen.2015.09.010

[35] F. Sarwar, S. Siddique, M. Younas, S.E.H. Gillani, M.M.z. Akram, B. Saleem, U. Mehmood, Materials Science & Engineering B, 314, 118013 (2025); https://doi.org/10.1016/j.mseb.2025.118013

[36] A. Shakeel, S.E.H. Gillani, Y.Q. Gill, M.H. Rasheed, R. Theravalappil, M. Younas, U. Mehmood, Journal of Physics and Chemistry of Solids, 192, 112087 (2024); https://doi.org/10.1016/j.jpcs.2024.112087